Journal of Thermal Analysis and Calorimetry, Vol. 88 (2007) 1, 83–86

INFLUENCE OF Ni CONTENT ON Fe–Nb–B ALLOY FORMATION

J. Bonastre, L. Escoda, A. González, J. Saurina and J. J. Suñol[*]

EPS, Campus Montilivi s/n. University of Girona, 17071, Girona, Spain

In this work three alloys, $Fe_{74}Nb_6B_{20}$, $Fe_{64}Ni_{10}Nb_6B_{20}$ and $Fe_{54}Ni_{20}Nb_6B_{20}$, were obtained by mechanical alloying to analyze the influence of Ni content on Fe–Nb–B alloy formation. Structural analysis by X-ray diffraction (XRD) confirms that partial substitution of Fe by Ni favours the formation during milling of a more disordered structure. Furthermore, thermal stability study was performed by differential scanning calorimetry (DSC) because thermally induced structural changes can affect soft magnetic behaviour. After 40 h of milling time, all DSC curves show several exothermic effects on heating associated to structural relaxation and crystallization. All alloys present a crystallization process with associated activation energy values ranged between 238 and 265 kJ mol^{-1} related to the crystalline growth of the bcc-Fe rich phase. In alloys with Ni, a second crystallization process appears at temperatures over 500°C with activation energies 397 (10% Ni alloy) and 385 kJ mol^{-1} (20% Ni alloy) probably associated to the nucleation and crystalline growth of a new phase.

Keywords: *Fe–Nb–B alloys, mechanical alloying, nanocrystalline materials*

Introduction

Developed by Benjamin and coworkers, mechanical alloying (MA) is an alternative technique in production of powder particles [1]. Being originally used in synthesis of oxide dispersion strengthened materials, mechanical alloying has been reported to be capable of producing alloys, intermetallic compounds, composites and nanocrystalline and amorphous materials [2–6]. During MA, powder particles are subjected to a severe mechanical deformation and are repeatedly deformed, cold-welded and fractured. Successive cold welding and fracturing enable powder particles to be always in contact with each other, resulting in clean surfaces and minimized diffusion distance [7].

Over the last decades, amorphous and more recently nanocrystalline materials have been investigated for applications in magnetic devices requiring magnetically soft materials [8]. Recently, Fe–X–B (*X*=Nb, Zr) based alloys with crystallite sizes less than 100 nm, have attracted attention due to some of their magnetic properties such as effective permeability and saturation magnetic flux density [9, 10]. These properties indicate that these materials may have application in magnetic parts and devices such as inductors, low and high energy frequency transformers, alternating current machines, motors, generators and sensors. Furthermore, nanocrystalline alloys with similar compositions have been obtained by mechanical alloying of elemental powder [11].

The substitution of small amounts of Co or Ni for Fe in Fe-based magnetic materials generally results in an increase of saturation magnetization [12, 13]. Among the different techniques to develop these materials, MA allows production of alloys in large quantities. In addition, MA powders can be compacted and consolidated to a complex shape [14]. In this study, several Fe(Ni)–Nb–B alloys were obtained and their structure and thermal behaviour were analyzed, including the influence of partial iron substitution by nickel. The milling time was chosen to obtain a disordered structure.

Experimental

Mechanical alloying was carried out in a planetary high-energy ball mill (Fritsch Pulverisette P7) starting from pure element powders: Fe (99.7% purity, particle size under 8 μm), Ni (99.8% purity, particle size under 7 μm), Nb (99.85% purity, particle size under 74 μm) and B (99.6% purity, particle size 50 μm). The nominal compositions of the produced and analyzed alloys were $Fe_{74}Nb_6B_{20}$, $Fe_{64}Ni_{10}Nb_6B_{20}$ and $Fe_{54}Ni_{20}Nb_6B_{20}$. The labels were 0% Ni, 10% Ni and 20% Ni, respectively. All the samples were milled at the same mill operation velocity (700 r.p.m.), in CrNi steel vials, and for 10, 20 and 40 h. The ball diameter was 12 mm, the ball-to-powder mass ratio was fixed at 5:1. The containers were sealed in a glove box with a stationary argon atmosphere.

* Author for correspondence: joanjosep.sunyol@udg.es

1388–6150/$20.00

Akadémiai Kiadó, Budapest, Hungary
Springer, Dordrecht, The Netherlands

The MA powders were thermally characterized by differential scanning calorimetry (DSC) in a Mettler-Toledo DSC822 equipment. Thermal evolution was performed under Ar atmosphere (flow rate: 40 mL min^{-1}) in isochronal scans. Furthermore, crystallization kinetics studied by working at different heating rates. X-ray diffraction (XRD) measurements were performed using a D-500 Siemens equipment, with CuK_α radiation, for phase identification and crystallite size determination.

Results and discussion

Thermal study was performed by differential scanning calorimetry. Figure 1 shows the DSC curves of the 0%-Ni alloy milled for 10, 20 and 40 h, respectively. Milling process was performed until 40 h in order to obtain a nanocrystalline or highly disordered alloy. X-ray diffraction patterns of the 0%-Ni alloy were given in Fig. 2. The peaks of bcc-Nb structure disappear after 20 h of MA indicating the formation of a bcc-Fe rich solid solution. Amorphous elemental B was introduced in the alloy in order to favour alloy formation and thermal stability. It is known that in Fe–B alloys with increased boron content an amorphous phase can be obtained at lower milling time [15]. Furthermore, in Fe–B rapidly solidified alloys, the higher the boron concentration the higher the crystallization temperature becomes [16]. This means that the thermal stability of the nanocrystalline phase increases when increasing boron concentration. After 40 h of milling time the nanocrystalline size of the bcc-Fe rich phase, as determined by X-ray diffraction analysis using the Rietveld method, was 8.1 nm. In essence, this nanoparticle size is close to where single-domain magnetic properties come into play [17].

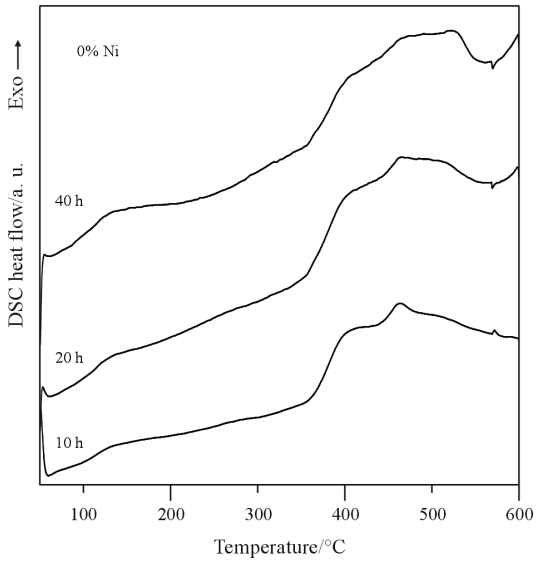

Fig. 1 DSC curves corresponding to the 0%-Ni alloy milled for: 10, 20 and 40 h. Heating rate: 10 K min^{-1}

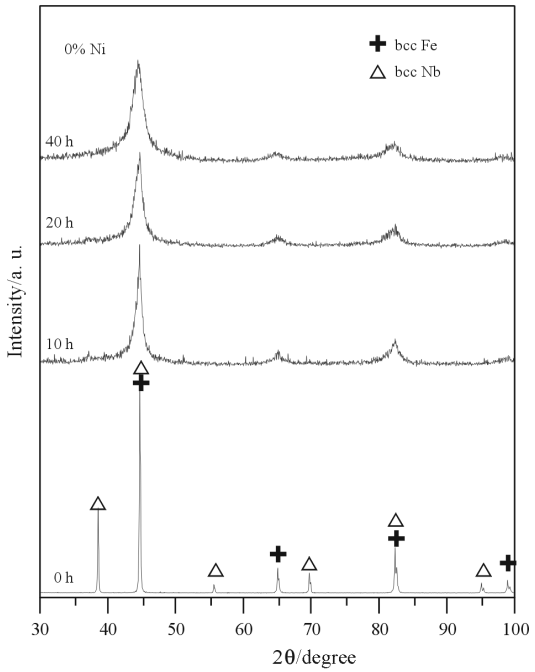

Fig. 2 XRD patterns of the 0%-Ni alloy: 0, 10, 20 and 40 h of MA

The general character of the DSC curves for all milling times are similar. The broad exothermic process starting at ~100–125°C might be due to early surface crystallization (particle surface) and/or internal stress [17, 18]. In all the curves, the main crystallization process is related to the crystalline growth of the bcc-Fe rich phase as detected in other alloys with similar composition [17]. The temperature broad effect detected by DSC corresponds to different Fe environments indicating the non-complete homogeneity of the alloy.

Thermal stability of the nanocrystalline phase is associated to higher activation energy and onset temperature of the crystalline growth process. The apparent activation energy, E, for the main crystallization process of alloys milled 40 h can be evaluated using the Kissinger equation [19] by linear fitting of $\ln(\beta/T_p^2)$ *vs.* $1/T_p$, being β the heating rate and T_p the assumed peak temperature (selected as the maximum value of the DSC curve). The crystallization data have been collected from DSC scans, run at different heating rates: 2.5, 5, 10, 20 and 40 K min^{-1}. The obtained value, 238±13 kJ mol^{-1}, can reasonably be associated with a grain growth process. The error, ~12%, indicates the correction of the peak temperature selection. We know from the literature, that the grain growth apparent activation energy of pure Fe is 174 kJ mol^{-1} for grain boundary diffusion and 251–282 kJ mol^{-1} for lattice diffusion [20]. However, the introduction of other elements to obtain a nanocrystalline alloy may

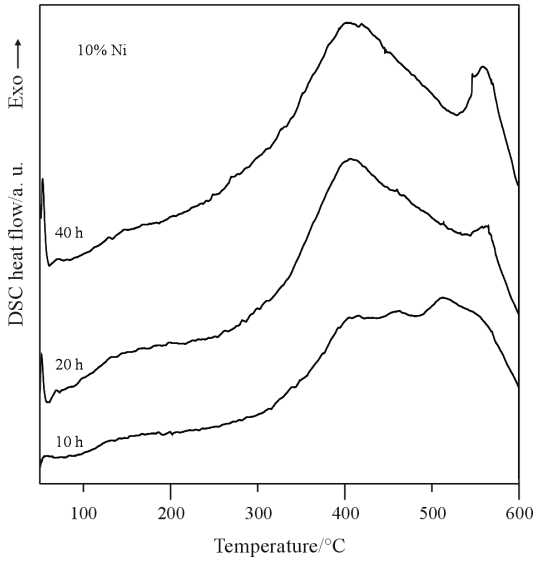

Fig. 3 DSC curves corresponding to the 10%-Ni alloy milled for: 10, 20 and 40 h. Heating rate: 10 K min^{-1}

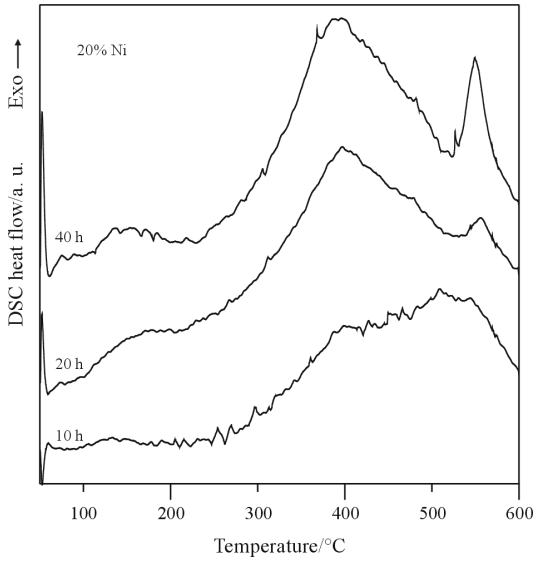

Fig. 4 DSC curves corresponding to the 20%-Ni alloy milled for: 10, 20 and 40 h. Heating rate: 10 K min^{-1}

increase/decrease this value. Energy values of 140 kJ mol^{-1} [21], 230 kJ mol^{-1} [22] and 290 kJ mol^{-1} [23] have been found in Fe–B based nanocrystalline alloys.

Among the modification of magnetic properties, it is known that the use of Ni favours the development of metastable structures at lower milling times [24]. For it, two additional MA processes with a partial Fe substitution by Ni were performed. Figure 3 shows the DSC scans corresponding to the 10%-Ni alloy. The DSC scan shape after 10 h of MA is similar to that of the alloy without Ni. Nevertheless, when increasing the milling time two clearly differentiated exothermic peaks appear. Kissinger analysis of the alloy milled for 40 h shows that their activation energies are 244±10 and 397±12 kJ mol^{-1}, respectively. The first process corresponds to the crystalline growth of the Fe-rich nanocrystalline phase perhaps favoured by lattice diffusion, and the narrow peak over 500°C probably corresponds to the nucleation and growth of a new crystalline phase. This is a typical behavior of Fe–Ni based alloys [25].

The DSC scans of the 20%-Ni alloy have a similar shape to those of the 10%-Ni alloy, as shown in Fig. 4. In this case, activation energies of the 20%-Ni alloy milled for 40 h are 265±10 and 385±11 kJ mol^{-1}. We can state that Ni introduction increases the activation energy associated to the crystalline growth of the bcc-Fe rich phase, but this process is moved to lower temperatures. In addition, a new crystalline process appears at temperatures over 500°C. Similar thermal behavior has been found in alloys with similar composition [26], where the last exothermic effect was associated to the formation of a new phase. Ulterior structural analysis of annealed samples is needed to confirm it.

From XRD patterns, see Figs 5 and 6 for the 10%-Ni and the 20%-Ni alloys, respectively, we can state that Ni introduction favours the formation of a highly disordered structure. After 40 h of MA, the 10%-Ni alloy is nanocrystalline, with a crystallite size of 5.3 nm, and the 20%-Ni alloy is like-amorphous. Nevertheless, from DSC analysis we obtain that at least a non-negligible amount of the alloy remains nanocrystalline.

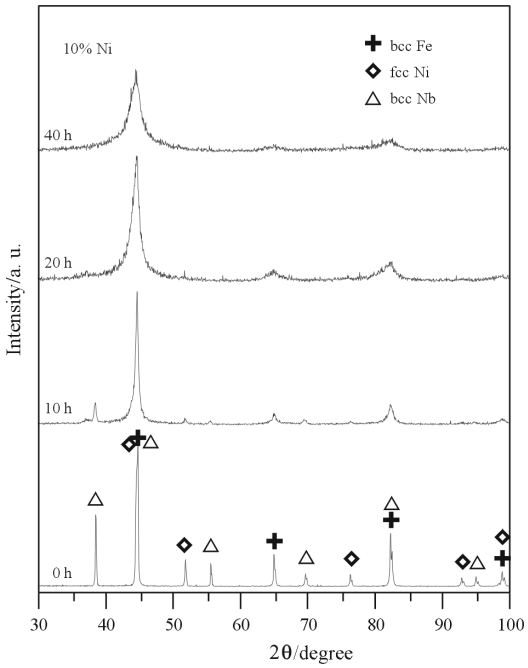

Fig. 5 XRD patterns of the 10%-Ni alloy: 0, 10, 20 and 40 h of MA

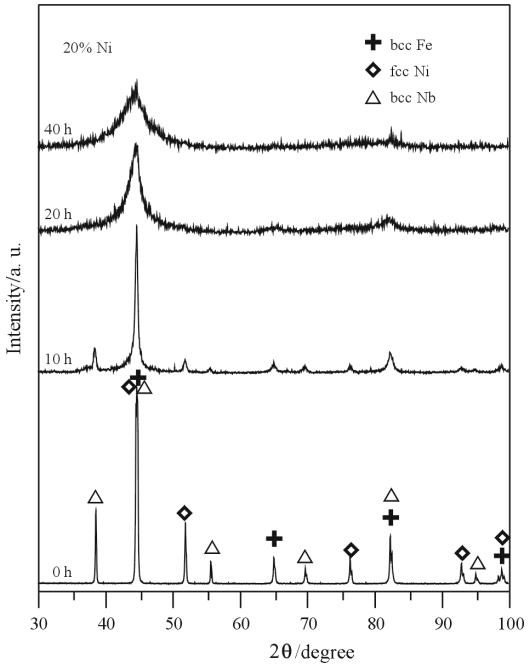

Fig. 6 XRD patterns of the 20%-Ni alloy: 0, 10, 20 and 40 h of MA

Conclusions

Three Fe based alloys, $Fe_{74-x}Ni_xNb_6B_{20}$ (x=0, 10 and 20), has been produced by mechanical alloying. The calorimetric data reveal a broad hump which starts at about 100–125°C and one/two crystallization zones at higher temperature. The hump is associated with the relief of internal stresses. The first crystallization process, detected in all alloys and with activation energy ranged between 238 and 265 kJ mol^{-1} is associated to the crystalline growth of the bcc-Fe phase and indicates the prevalence of lattice diffusion over grain boundary diffusion. A second crystallization process appears in alloys with Ni at temperatures over 500°C. The partial substitution of Fe by Ni produces an increase of the activation energy associated to the crystalline growth of the bcc-Fe rich phase, but this process is moved to lower temperatures. Furthermore, from XRD analysis we can state that Ni introduction favours the formation of a highly disordered structure. After 40 h of MA, the 10%-Ni alloy is nanocrystalline, with a crystallite size of 5.3 nm, and the 20%-Ni alloy is like-amorphous, whereas the 0%-Ni alloy has a crystallite size of 8.1 nm.

Acknowledgements

Financial support from MICYT MAT2003-08271-C02-02 and MAT2006-13925-C02-02 (FEDER) and DURSI 2005-SGR-00201 is acknowledged. J. B. agrees a Spanish FPI fellowship.

References

1 J. S. Benjamin, Metall. Trans., 1 (1970) 2943.
2 T. Nasu, K. Nagaoka, N. Itoh and K. Suzuki, J. Non-Cryst. Solids, 122 (1990) 216.
3 C. C. Koch, Nanostruct. Mater., 2 (1993) 109.
4 N. Z. Lyakhov, T. F. Grigorieva and A. P. Barinova, J. Therm. Anal. Cal., 82 (2005) 719.
5 J. J. Suñol, A. González, L. Escoda and A. Vilaró, J. Therm. Anal. Cal., 80 (2005) 257.
6 K. Wieczorek-Ciurowa and K. Gamrat, J. Therm. Anal. Cal., 82 (2005) 719.
7 C. Suryanarayana, Prog. Mat. Sci., 46 (2001) 1.
8 M. E. McHenry, M. A. Willard and D. E. Laughlin, Prog. in Mater. Sci., 44 (1999) 291.
9 M. Kopcewicz, A. Grabias and D. L. Williamson, J. Appl. Phys., 82 (1997) 1747.
10 J. S. Garitaonandia, P. Gorria, L. Fernández Barquín and J. M. Barandiarán, Phys. Rev., B, 26-9 (2000) 6150.
11 C. Stiller, J. Eckert, S. Roth, R. Schafer, U. Klement and L. Schultz, J. Non-Cryst. Solids, 207 (1996) 620.
12 D. Wexler, R. Bennett, M. Emr and K. P. Gillerad, Mater. Sci. Forum, 235–238 (1997) 729.
13 Y. I. Jang, J. Kim and D. H. Shin, J. Mater. Sci. Eng. B, 78 (2000) 113.
14 S. Linderoth and S. Morup, J. Appl. Phys., 69 (1991) 5256.
15 A. Calka and A. P. Radlinski, Mater. Sci. Eng. A, 134 (1991) 1350.
16 T. Nakajima, I. Nagami and H. Ino, J. Mater. Sci. Letters, 5 (1986) 60.
17 A. Calka and A. P. Radlinski, Acta Metall., 35 (1987) 1823.
18 M. T. Clavaguera-Mora, J. J. Suñol and N. Clavaguera, Mater. Sci. Forum, 360 (2001) 459.
19 H. Kissinger, Anal. Chem., 29 (1957) 1702.
20 T. R. Malow and C. C. Koch, Acta Mater., 45 (1997) 2177.
21 Y. J. Liu, I. T. H. Chang and P. Bowen, Mater. Sci. Eng., A304–306 (2001) 383.
22 R. S. de Biasi and M. L. N. Grillo; J. Alloys Compd., 279 (1998) 233.
23 J. J. Suñol, A. González and J. Saurina, J. Therm. Anal. Cal., 72 (2003) 329.
24 J. J. Suñol, N. Clavaguera and M. T. Mora, J. Non-Cryst. Solids, 287 (2001) 114.
25 J. J. Suñol, T. Pradell, N. Clavaguera and M. T. Clavaguera-Mora, Mater. Sci. Forum, 360 (2001) 525.
26 A. González, J. J. Suñol, J. Bonastre, L. Escoda and J. Caleya, J. Therm. Anal. Cal., 80 (2005) 253.

DOI: 10.1007/s10973-006-8092-2